Epoxy/Nano-Silica Composites: Curing Kinetics, Glass Transition Temperatures, Dielectric, and Thermal–Mechanical Performances

Yun Zheng,[1,2] Kim Chonung,[1,2] Genlin Wang,[1,2] Ping Wei,[1,2] Pingkai Jiang[1,2]

[1]*School of Chemistry and Chemical Engineering, Shanghai Jiao Tong University, Shanghai 200240, People's Republic of China*
[2]*Shanghai Key Lab of Electric Insulation and Thermal Aging, Shanghai 200240, People's Republic of China*

Received 28 May 2008; accepted 24 June 2008
DOI 10.1002/app.28875
Published online 17 October 2008 in Wiley InterScience (www.interscience.wiley.com).

ABSTRACT: Nano-silica particles were employed for enhancement of epoxy vacuum pressure impregnating (V.P.I.) resin. The influences of nano-silica particles on the curing reaction, glass transition temperatures, dielectric behavior, and thermomechanical performances were investigated. The activation energy (*E*) for the epoxy curing reaction was calculated according to Kissinger, Ozawa, and Friedman-Reich-Lev methods. The glass transition temperatures were determined by means of differential scanning calorimetry, dynamic mechanical analysis, dc conduction, and ac dielectric loss analysis. Relationships between the glass transformation behaviors, the thermomechanical performances, and the dielectric behaviors were discussed. The influences of nano-silica particles on the mechanical properties were also discussed in terms of non-notched charpy impact strength and flexural strength. The morphologies were studied by means of SEM and TEM. The results indicated that nano-silica particles could effectively increase both the toughness and strength of epoxy resin at low loadings (no more than 3 wt %) when nano-silica particles could be well dispersed in epoxy matrix without any great aggregations. © 2008 Wiley Periodicals, Inc. J Appl Polym Sci 111: 917–927, 2009

Key words: epoxy resin; nano-silica particle; glass transition temperature; dielectric behavior; enhancement

INTRODUCTION

Epoxy resin is one of the most important thermosetting plastics and is widely used as insulating materials in electrical and electronic applications, e.g., dry type transformers and rotating machines for their excellent mechanical and electrical properties.[1–3] However, the application of epoxy resins is sometimes constrained owing to their high viscosity and poor impact resistance. Nowadays, as the working voltage, the power per unit volume, the working temperature, and the geometrical dimensions of electrical insulation systems have all greatly increased, the insulating materials used in power electronics are subjected to severer thermal, electrical, ambient, and mechanical stresses (called as TEAM stresses).[2,4] And also, the requirement of reducing the insulation thickness of the electrical and electronic apparatuses has been considered to be of great significance for the sake of realizing the more compact structures of the insulation systems. The modification of epoxy vacuum pressure impregnating (V.P.I.) resin aiming at improving the processability, toughness, as well as the mechanical and dielectric strength is quite necessary to meet such higher requirements pertinent to the process technology and the operating reliability of the insulation systems.

The toughening agents commonly applied in epoxy resin, however, often sacrifice other properties such as strength, thermomechanical properties or heat resistance. Such tougheners include, for example, reactive liquid rubbers, core shell particles, glass beads, microvoids, and their combinations.[1,5] Recently, toughening modification of epoxy resin with the incorporation of inorganic nanoparticles has attracted great attentions because they provide low shrinkage, good thermal stability, and excellent toughness without causing great reduction in mechanical strength at relatively low concentrations.[5–10] For example, it has been demonstrated that both Young's modulus and fracture toughness of epoxy can be improved by the incorporation of layered silicates.[11–13] Zilg et al.[12] reported that the exfoliated structures mainly improve the stiffness of the epoxy matrix, and the remaining stacked structures of intercalated clay platelets can improve the toughness. The

Correspondence to: Y. Zheng (carolzy@sjtu.edu.cn) or P. Jiang (pkjiang@sjtu.edu.cn).

Contract grant sponsor: Shanghai Science and Technology Commission, China; contract grant number: 05dz22303.

© 2008 Wiley Periodicals, Inc.

performances of nanocomposites are greatly affected by both the properties of the epoxy matrix and the nano particles, as well as their interfaces, and the dispersion of the nano particles in the matrix. With the incorporation of special functionalized fillers, specific properties can be improved or achieved. For instance, alumina trihydrate and layered silicate can be used to improve the fire retardancy.[14] Some iron oxides might be used for improvement of magnetic properties,[15,16] zinc oxide to develop active materials exhibiting the behaviors of a nonlinear resistivity, and epoxy/silica nano-composites have been used as the electronic insulating and optical packaging materials because of their superior mechanical and electrical properties.[17,18]

In our study, nano-silica was applied in the epoxy V.P.I. resin, aiming at improvement of strength and toughness with no great impairment to insulating properties and thermal stabilities. (3-Glycidoxypropyl)methyldiethoxysilane (GPMDS) was employed as a diluent to reduce the viscosity for the room temperature impregnating technique. At the same time, it is expected that GPMDS can act as coupling agent to improve the compatibility of nano-silica particles and the epoxy resin. The influences of nano-silica on the curing reaction, glass transition behavior, dielectric properties, and mechanical performances of the epoxy resin were investigated at the same time.

EXPERIMENTAL

Materials and sample preparation

Materials

The epoxy used was a commercial grade of 3, 4-epoxycyclohexylmethy-(3′, 4′-epoxy)cyclohexane carboxylate (CYRACURE UVR-6105, from DOW Chemical Company) with an epoxy equivalent weight of 126–135 g/mol. The hardener was methyl-hexahydrophthalic anhydride (MHHPA), obtained from Lon ca group, Italy. Neodymium (III) acetylacetonate trihydrate ($Nd(acac)_3$) was used as latent catalyst and purchased from Aldrich Chemicals Inc. GPMDS was purchased from GE chemicals. The nano-silica used for reinforcement was obtained from High Technology Nano Company, Nanjing, China, which contains silica spherical particles with average diameter of 20 nm, and without any surface treatment.

Sample preparation and curing

The stoichiometric proportion of epoxide and anhydride was controlled at 1 : 0.85, and the catalyst concentration is 0.3 parts in per 100 parts epoxy resin. The content of GPMDS was 15 parts per 100 parts epoxy resin. The loading concentrations of Nano-silica particles were 0 wt % (the control epoxy resin), 1, 2, 3, and 5 wt %, respectively.

Nano-silica particles were dried at 200°C in vacuum for 15 h and then cooled to room temperature in vacuum prior to use. The dried nano-silica particles were dispersed in analytically pure acetone by applying ultrasonic vibration for 30 min at room temperature. At the same time, the required quantity of $Nd(acac)_3$ was added to the epoxy resin, stirred, and degassed at 150°C in a three-necked flask. The temperature was then lowered down to room temperature when a homogeneous solution with tint orange color was obtained. Afterward, the solution of epoxy resin/Nd $(acac)_3$ was mixed with the solution of nano-silica/acetone by mechanical agitation and sonication for 30 min. The resulting mixture was heated to 80°C, mechanically agitated and degassed for 1 h to remove the acetone. Subsequently, MHHPA and GPMDS at designed ratios were added under vigorous mechanical stirring and degassed for 30 min. The final mixture was then poured onto preheated stainless steel molds, precured in an oven at 135°C for 3 h, followed by postcure at 160°C for 14 h. The molds were left in the oven and allowed to cool gradually to room temperature.

CHARACTERIZATION

Curing kinetics

The calorimetric measurements were done using a Perkin–Elmer Pyris 1 differential scanning calorimeter in a dry nitrogen atmosphere with a flow rate of 20 mL/min. The instrument was calibrated with standard Indium. The sample weight was around 5 mg. Dynamic differential scanning calorimetry (DSC) analysis was performed in the temperature range of 25–320°C at five different heating rates of 5, 10, 15, 20, and 25°C/min.

The kinetic model for a dynamic curing process with a constant heating rate can be expressed in the following form[19,20]:

$$r = \frac{d\alpha}{dt} = k(T)f(\alpha) = A\exp(-E/RT)f(\alpha) \quad (1)$$

where r is the reaction rate; α is the conversion; t is time; $k(T)$ is the rate constant dependent on the temperature T and may be described by the Arrhenius expression $k(T) = A\exp(-E/RT)$; A is the pre-exponential factor; E is the activation energy; and R is the gas constant. The activation energy (E) can be determined as follows:

According to Kissinger's equation,[20–22]

$$-\ln(\beta/T_p^2) = \ln(E/RAn) - (n-1)\ln(1-\alpha_p) + E/RT_p \quad (2)$$

In a dynamic curing, the plot of $-\ln(\beta/T_p^2)$ against $1/T_p$ will be a straight line with a slope of E/R, where T_p is the temperature corresponding to the exothermic peak, and β is the heating rate.

According to Ozawa's method,[20,22,23]

$$\log\beta = (1/2.303)\ln\beta = -0.4567\,(E/RT_p) + [\log(AE/R) - \log F(\alpha) - 2.315] \quad (3)$$

Based on this method, a plot of ln β against $1/T_p$ should be a straight line with a slope of $-(2.303 \times 0.4567)E/R$.

Both Kissinger's and Ozawa's methods are known to analyze the overall curing process and can determine an average value of the activation energy E. Another method based on Friedman-Reich-Lev approach[24] allows the activation energy to be determined as a function of the extent of conversion α.[20,25,26] By taking the logarithm of both sides of eq. (1), a linear expression for the logarithm of cure rate can be obtained,

$$\ln\left(\frac{d\alpha}{dt}\right) = \ln A + \ln(f(\alpha)) + \left(-\frac{E}{R}\right)\frac{1}{T} \quad (4)$$

Therefore, the reaction rate is only a function of temperature at any given conversion, and the plot of $\ln(\frac{d\alpha}{dt})$ against $1/T$ should be a straight line with slope $-E/R$ which could be used to calculate the activation energy.

The glass transition temperature and dielectric behavior

The glass transition temperatures (T_gs) of the epoxy/nano-silica composites were obtained by DSC, dynamic mechanical analysis (DMA), dc conduction, and dielectric analysis to probe molecular mobility in different ways:

The T_g values were primarily obtained by DSC measurements (Perkin–Elmer Pyris 1 calorimeter) in the temperature range of 25–300°C at a heating rate of 20°C/min. The glass transition temperature was taken as the midpoint of the capacity changes during the heating process.

DMA measurements were carried out using equipment from TA instrument (DMA 2980) in flexural bending mode at a frequency of 1 Hz with the specimen dimensions of 50 mm × 15 mm × 3 mm. A peak-to-peak deformation of 20 μm was selected. The experiments were carried out from the ambient temperature to 280°C at a heating rate of 5°C/min. DMA determines storage moduli and tan δ peak.

A digital high-resistance meter (6517A, Keithley, USA) was used to investigate the changes of dc conductivity with the increase of temperature.

Dielectric dissipation loss tangent was obtained using a Schering bridge (TETTEX AG Instrument, Switzerland) over the temperature range of 25–240°C at a frequency of 50 Hz.

Mechanical performances

The flexural tests were performed with an Instron series IX 4465 materials tester in three-point bend mode according to ASTM D 790, at a crosshead speed of 2 mm/min. Specimens of 80 mm × 15 mm × 4 mm were used for the measurements. Ten specimens for each sample were used for the tests. The arithmetic mean of all values obtained was taken as the flexural strength.

The non-notched charpy impact tests were performed according to ASTM E 23 in a Rayran impact tester. Non-notched specimens of 80 mm × 10 mm × 4 mm were tested at a hammer speed of 2.9 m/s and pendulum weight of 0.238 kg. Ten specimens for each sample were used for the tests. The arithmetic mean of all values obtained was taken as the impact strength.

Morphology analysis

The morphologies of the cured epoxy/nano-silica composites were observed on the impact fractured surfaces with field emission scanning electron microscopy (FE-SEM, JEOL JEM-4701, Tokyo, Japan). Bright field transmission electron microscopy (TEM, JEOL JEM-100SX) was used to analyze the dispersion of the nano-silica particles in the epoxy matrix. TEM specimens were cut using an ultramicrotome (Ultracut-1, UK) with a diamond knife, and TEM images were obtained with an acceleration voltage of 100 kV.

RESULTS AND DISCUSSIONS

Influences of nano-silica particles on the curing reaction

Figure 1 shows the dynamic DSC curves at five heating rates of 5, 10, 15, 20, and 25°C/min for epoxy/nano-silica composites. It is seen in Figure 1 that the starting and ending points of the exothermic peaks shift to higher temperatures at the higher heating rates. Accordingly, the maximum heat flow and the exothermal peak temperature also increased. It is also observed that the control epoxy resin exhibits a sharp and strong exothermic peak with a very small shoulder peak at the onset position. Differently, in the epoxy/nano-silica composites, two separate exothermic peaks are observed: a very small one at lower temperatures and a strong one at higher temperatures. Besides, with the incorporation of nano-silica particles, the exothermic peaks are found to become blunt, and the height of the peaks decrease with the increase of nano-silica particles

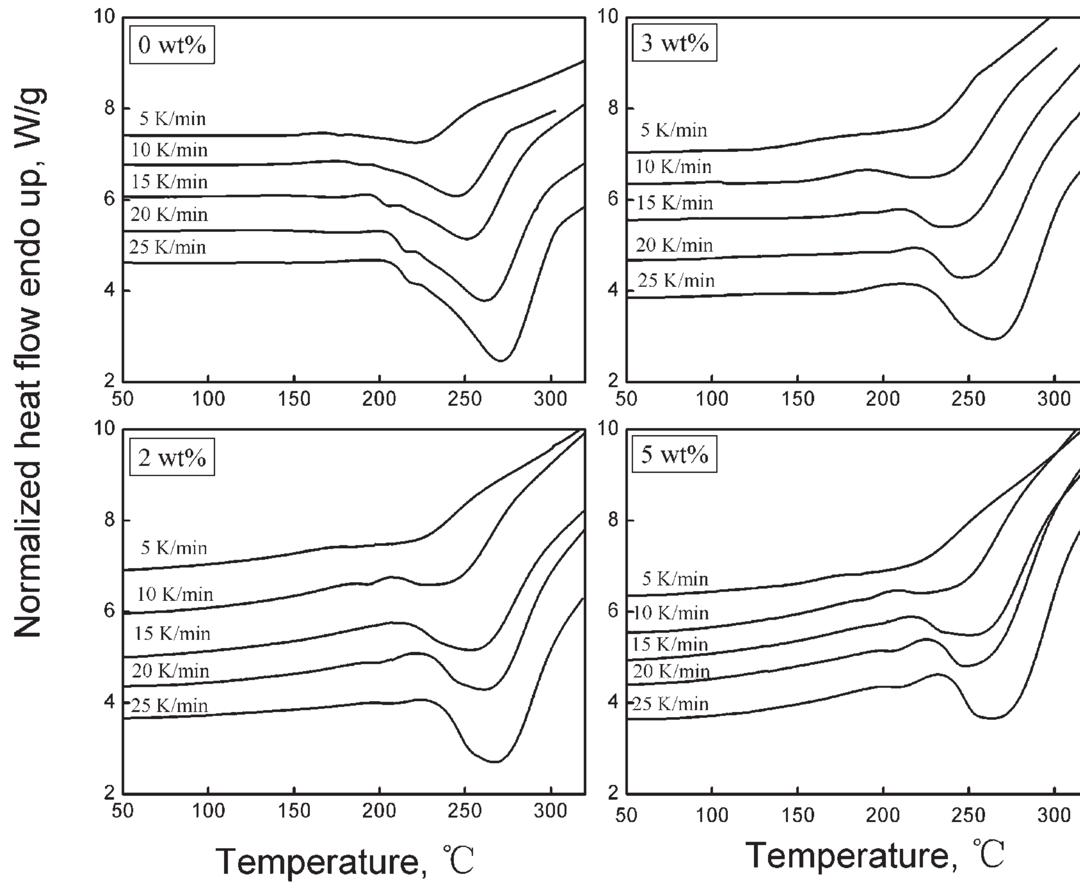

Figure 1 Nonisothermal DSC curves at different heating rates for epoxy/nano-silica composites.

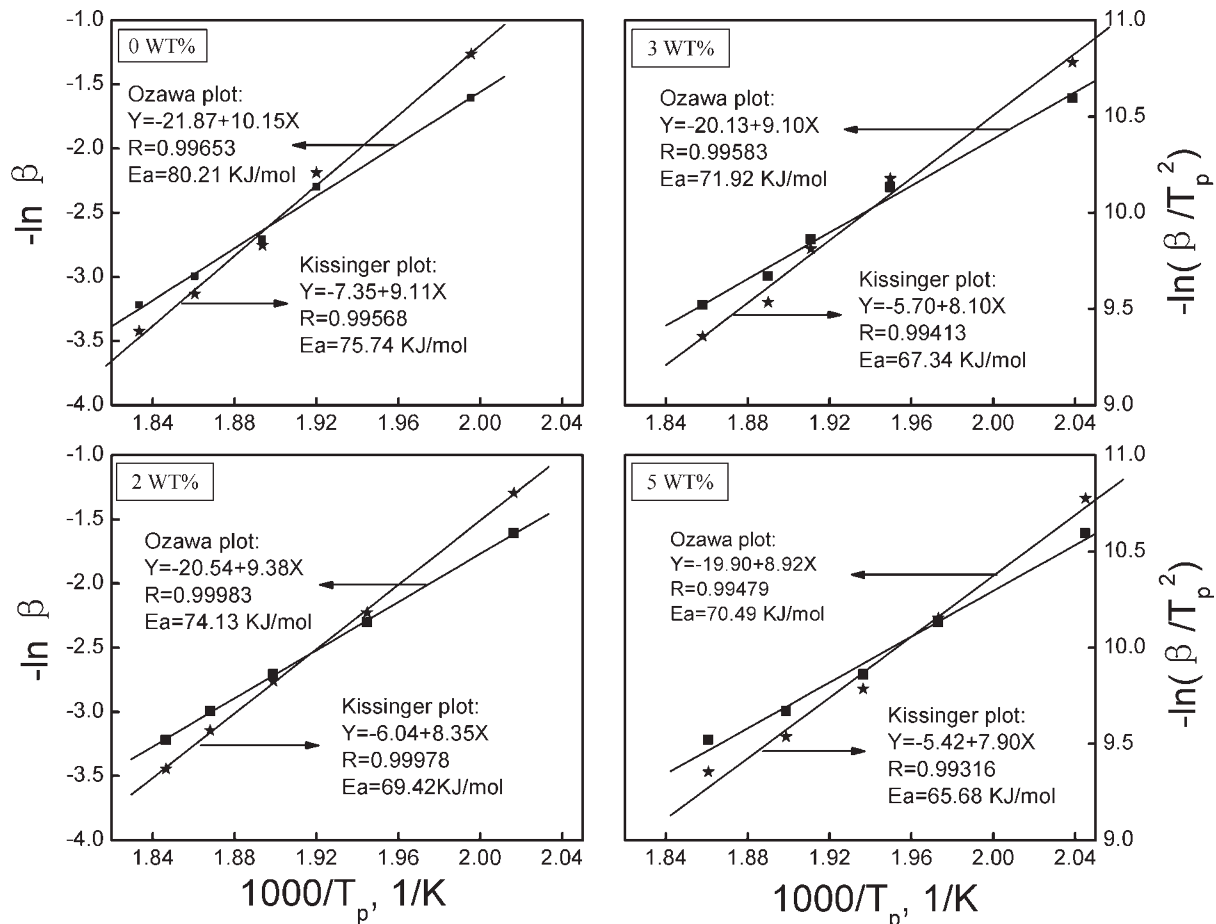

Figure 2 Kissinger's and Ozawa's plots for epoxy/nano-silica composites.

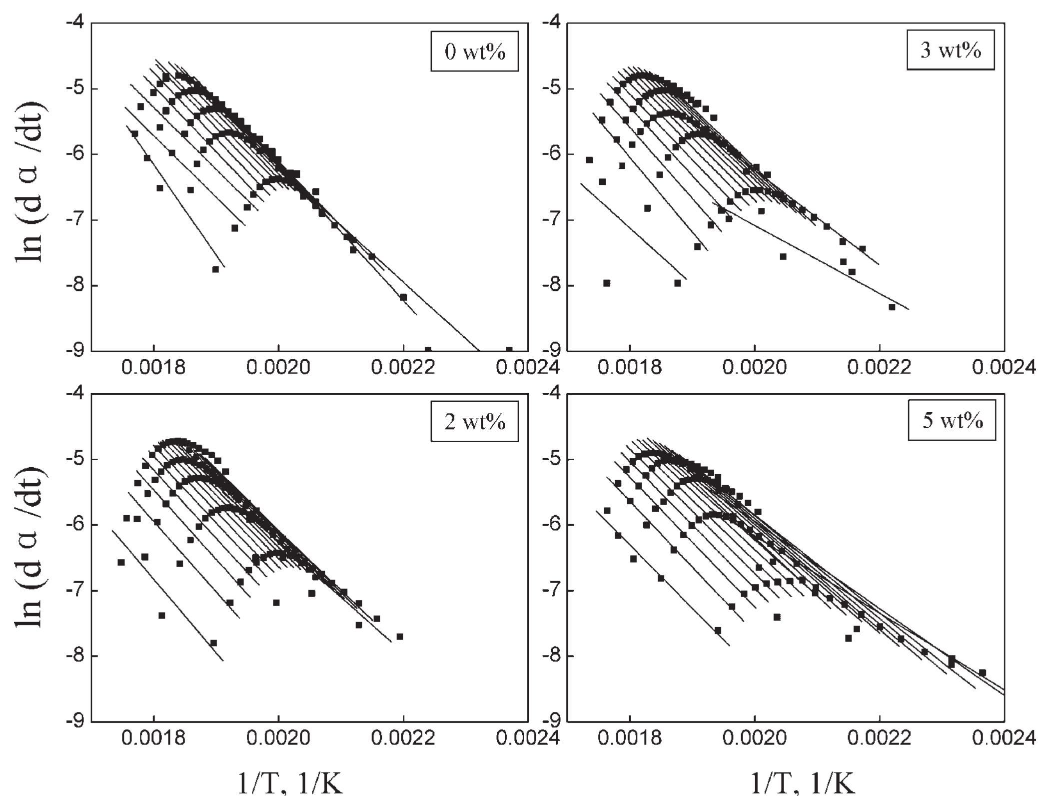

Figure 3 The plots of ln ($d\alpha/dt$) against $1/T$ according to Friedman-Reich-Lev method.

concentrations, which indicates relatively slow reaction rate in epoxy/nano-silica composites. It is also worthy of mentioning that in the epoxy/nano-silica composites, a broad and weak exothermic peak is also observed at low temperatures of about 50–180°C although it is not easy to discriminate. Such an exothermic peak cannot be seen in the DSC curves for the control epoxy resin. This indicates that in the epoxy/nano-silica composites, the curing reaction initiates much easier than that in the control epoxy resin, which may be attributed to the existence of the —OH groups on the surface of the nano-silica particles.

Figure 2 shows the plots and the calculated activation energies determined by Kissinger's and Ozawa's methods. The calculated activation energies for epoxy resin containing of 0, 2, 3, and 5 wt % nano-silica are 80.2, 74.1, 71.9, 70.5 KJ/mol, respectively, by Ozawa's method and 75.7, 69.4, 67.3, 65.7 KJ/mol by Kissinger's method. As can be seen, although the values obtained from the two different methods are slightly different from each other, both Kissinger's and Ozawa's methods give a decreased value of activation energy for epoxy resin with the increasing nano-silica loadings.

Figure 3 shows the plots of $\ln\left(\frac{d\alpha}{dt}\right)$ against reciprocal absolute temperature according to the method based on Borchardt and Daniels approach. Figure 4 shows the plots of activation energies against conversions for the epoxy resin obtained from the straight lines shown in Figure 3. As can be seen, the activation energies of epoxy/nano-silica composites are lower than that of the control epoxy resin. This is in agreement with the results obtained by the Kissinger's and Ozawa's methods. The decrease in activation energy with the incorporation of nano-silica may be attributed to the introduction of —OH

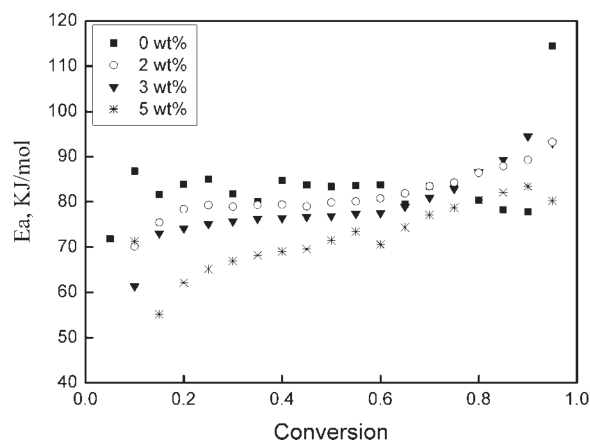

Figure 4 The plots of activation energy (E) as a function of conversion.

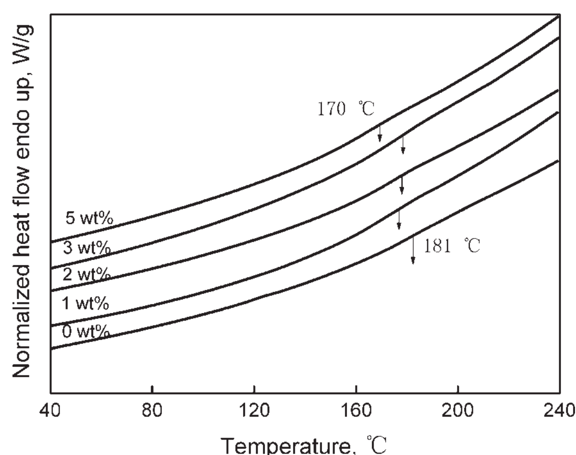

Figure 5 DSC scans on the fully cured epoxy/nano-silica composites.

groups which are adhered to the surface of nano-silica particles into epoxy resin.

The glass transformation process, thermomechanical performances, and dielectric behaviors

The glass transformation process is a common and important phenomenon of polymers, which is known to accompany the changes of many physical properties of polymers, e.g., the heat capacity, modulus, conductivity, and dielectric relaxation, etc.[27,28] All these changes are related to the mobility of the segmental chains and can reflect the movements and interactions of polymer chains. Amorphous polymers are hard and brittle at temperatures below T_g, whereas when heated to temperatures above T_g, they become elastic like rubber or liquefy depending on their molecular structures.[27] Some polymeric materials, which exhibit excellent insulating properties at temperatures below T_g, might show the semiconducting characteristics at temperatures above T_g.[4] Therefore, the study and measurement of the glass transition temperatures of polymers are very important.

The T_g values of epoxy resins measured by DSC are around 180°C as shown in Figure 5. It is observed that even though the T_g does not simply decrease with the increase of nano-silica concentration, it is apparent that the epoxy/nano-silica composites display close but lower T_gs than that of the control epoxy resin. The T_g values obtained by DMA measurements are very close to those by DSC. The dynamic mechanical spectra of the epoxy/nano-silica composites are shown in Figure 6. In the plots of tan δ as functions of temperature, the peak at about 180°C can be assigned to the glass rubber transition of epoxy resins. It can be seen that there are neglectable slight differences between the T_g of the control epoxy resin and the epoxy/nano-silica composites. And also, there are slight depressions of T_g in the epoxy/nano-silica composites with the nano-silica loadings of 1 and 2 wt %, whereas the tendencies of slight increase are observed in those of 3 and 5 wt %. It is worth noticing that the tan δ peak values of epoxy/nano-silica composites are lower than that of the control epoxy resin, which may be possibly because that the polymer chain segments in the epoxy/nano-silica composites are separated away by the nano-silica particles and are subjected to smaller frictional resistance when moving.

The storage moduli of epoxy/nano-silica composites are found to be higher than that of the control epoxy resin. In the nano-silica composites, the nano-silica particles are homogeneously dispersed in the epoxy matrices and the increased modulus may be attributed to the nano-reinforcement effect of the nano-silica particles on epoxy matrix. Nonetheless, it is noted that the moduli of the nano-composites do not exhibit the monotonous increment as a function of nano-silica concentration although all the nano-composites investigated possess increased storage modulus in glassy state. The supposed explanation for this observation can be done on the basis of the two opposing effects of nano-silica on the matrices of the materials: On the one hand, the nano-

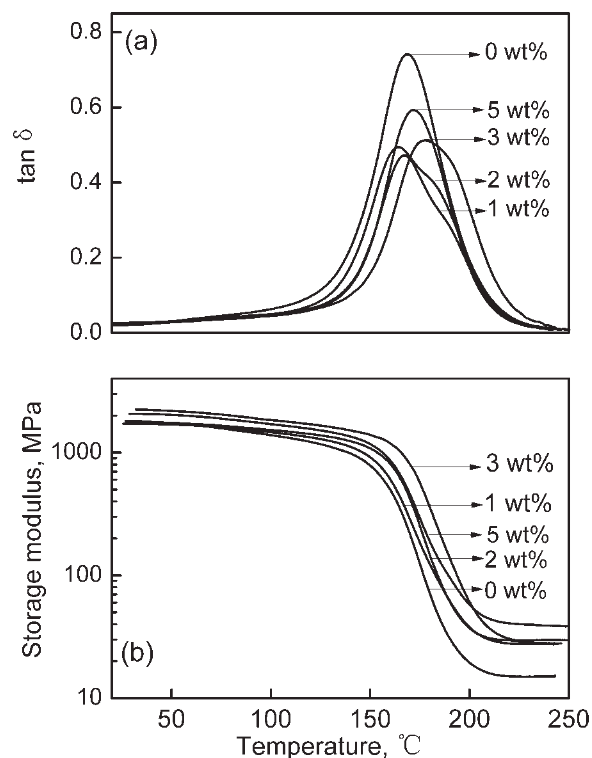

Figure 6 The dynamic mechanical spectra of (a) tan δ and (b) storage modulus for the epoxy/nano-silica composites.

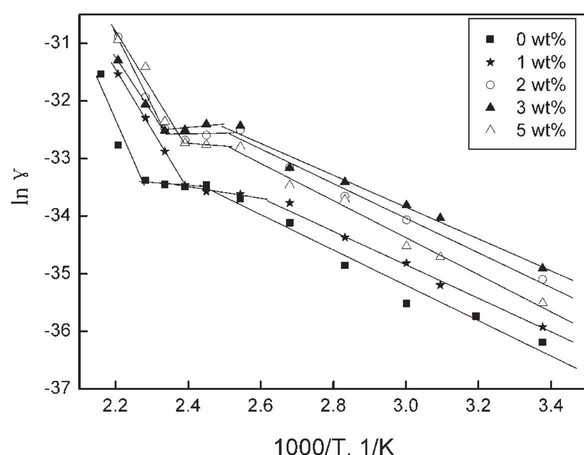

Figure 7 The plots of ln γ versus 1000/T for epoxy/nano-silica composites at 600 s from the dc voltage application.

reinforcement effect of nano-silica particles on polymer matrix can result in the increase of modulus of the nanocomposites. On the other hand, the aggregations of the nano-silica particles can induce the decrease in modulus for the nanocomposites, especially at higher concentrations of nano-silica particles. And the storage moduli of rubbery plateau for the epoxy/nano-silica composites are also higher than that of the control epoxy resin. The moduli of rubber plateau for polymer networks are generally related to the crosslinking density of the materials.[29] In the epoxy/nano-silica composites, nano-silica particles are expected to act as physical crosslinkers.

The plots of the natural logarithm of conductivity (ln γ) as a function of reciprocal absolute temperature ($1/T$) are shown in Figure 7. It can be observed that the graph showing the dependence of (ln γ) on the value of ($1/T$) consists of two rectilinear portions with different angles of inclination and one short plateau between them. Such temperature dependences of dc conductivity for epoxy/nano-silica composites can be well interpreted in terms of the ionic conduction mechanism. In the cured epoxy resin, the ionic conductivity γ can be expressed as: $\gamma = nqu$, where n is the ion density per unit volume of the medium, q is the charge amount of an ion, u is the mobility of charge carriers. Under invariable electric field, u is determined by the thermal activity of the ions and the interactions of the medium on the ions.[4]

At temperatures far below T_g, the interaction between macromolecules is quite intensive, and no increase of ion density in the cured epoxy system can be expected. Thereby, the behavior of dc conductivity for the cured epoxy system can be considered to be dependent mainly on the change of the thermal activity of the ions. In other words, at temperatures below T_g, the thermal activities of the ions increase slowly with the increase of temperature, resulting in low γ values which increase slowly with temperature. The short plateau may be related to the glass transformation process. Above the glass transition temperature T_g, the temperature is high enough to generate new free and/or semifree ions in the cured epoxy system that the ion density becomes higher and higher together with the greatly increased mobility of ions as the temperature increases, which causes the quick increase of dc conductivity.

It can also be observed from Figure 7 that the conductivity of the epoxy/nano-silica composite increases with the increase of the nano-silica loadings. This is because that the nano-silica particles were used without any surface treatment and a large amount of —OH and impurities might be adhered on the surface of nano-silica particles which were introduced into the epoxy composites, resulting in higher conductivity.

The influence of nano-silica particles on the dielectric loss tangent (tan δ) is shown in Figure 8. It is observed that the temperature dependences of tan δ for the epoxy/nano-silica composites exhibit typical "dipole maximum." In epoxy/nano-silica composites, the dielectric loss in ac electric field can be considered to be attributed both to the relaxation loss due to the motion of electric dipoles and the conduction loss due to the motions of ionic impurities.

Considering the temperature dependence of the relaxation time, the dielectric loss due to the relaxational polarization may be expressed as[30]:

$$\tan\delta = \frac{(\varepsilon_s - \varepsilon_\infty)\omega\tau(T)}{\varepsilon_s + \varepsilon_\infty[\omega\tau(T)]^2} \tag{5}$$

where ε_s and ε_∞ are the static and optical permittivities, respectively; ω is the angular frequency; $\tau(T)$ is

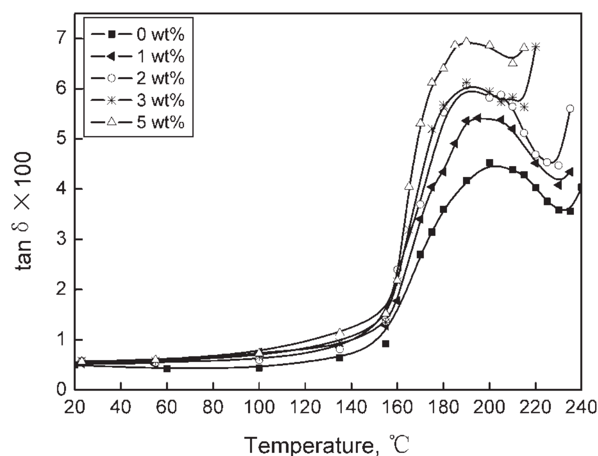

Figure 8 The plots of the dielectric loss tangent (tan δ) as a function of temperature for epoxy/nano-silica composites (the measuring frequency is 50 Hz).

the relaxation time of a dielectric polarization as the function of temperature.

The dielectric losses caused by the dielectric relaxational polarizations reach their maximum at temperatures close to T_g. At temperatures far below T_g, the polar groups are attached tightly to the polymer chains, and the motions of segmental chains are "frozen," which can cause the very long relaxation times and very low values of tan δ. When the temperature is close to T_g, the motions of segmental chains become easier and easier, resulting in the increase of the dielectric loss, whereas beyond T_g the chaotic thermal motions of the dipoles again give an obstacle to their orientations toward the external electric field, again leading to a decrease in the dielectric loss. Except for the dielectric loss due to the dipole polarization, the interfacial polarization occurring at the interfaces between the different dielectric media and/or at the interfaces between the metal electrode and the insulation may be more or less contributed to the dielectric loss behaviors around the glass transition temperature because the measuring frequency used is as low as 50 Hz.

And also, it can be observed that the dielectric loss pertaining to the ionic conduction predominates over that due to the relaxational polarization at temperatures above the glass transition temperature. Considering the temperature dependence of dc conductivity, the dielectric loss owing to electrical conduction can be depicted as[4,30]:

$$\tan\delta = \frac{A}{\omega\varepsilon_0\varepsilon}\exp\left(\frac{-B}{T}\right) \quad (6)$$

It can be concluded that the temperature dependences of dielectric loss mentioned earlier also strongly support the explanation of the γ–T behaviors for the cured epoxy systems investigated in this study.

It should be also noted that compared with the control epoxy resin, there are no obvious changes in the temperature corresponding to the location of the peak related to the glass transition position for epoxy/nano-silica composites. This demonstrates that the incorporation of nano-silica particles into epoxy has slight influence on the crosslinking density. However, the increase of the nano-silica particle loadings in epoxy causes an increase in the peak values of tan δ. This may be attributed to the increasing ionic impurities due to the introduction of —OH groups into epoxy resin by nano-silica particles.

It is noteworthy that the T_g values obtained from the different measurements are different from one another: The T_g values determined from the conductivity measurement, DSC, and DMA analysis, and dielectric loss measurement are observed to be around 150, 180, and 200°C, respectively. Such differences may be ascribed to the differences in test frequency and heating rate of individual methods used.

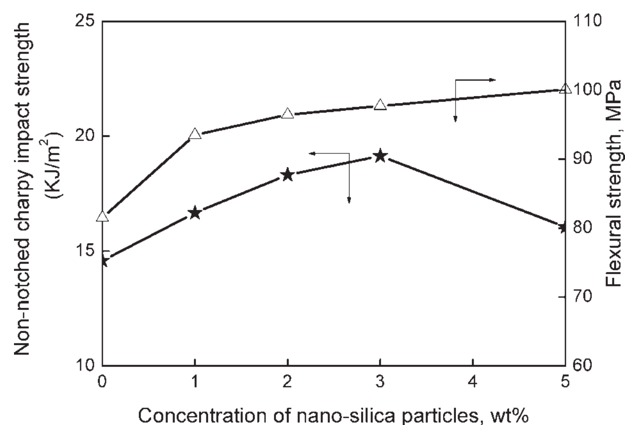

Figure 9 The mechanical properties of epoxy and epoxy/nano-silica composites.

Enhancement and morphologies

The enhancement effect of nano-silica loadings on epoxy resin is shown in Figure 9. It is revealed that the nano-silica addition is effective to reinforce the epoxy resin. It can be observed that epoxy with low nano-silica loadings (less than 3 wt %) exhibits obviously increased flexural strength than the control epoxy resin, and more addition of nano-silica particles than 3 wt % causes slight and neglectable increment in flexural strength. The impact strength increases with the increasing loading of nano-silica particles, reaching a maximum at 3 wt %, and further addition of nano-silica leads to a reduction in impact strength. The significant enhancement effect can be proved and explained by the morphology of the fractured surfaces shown in Figure 10. In the case of the control epoxy (series "a"), the fractured surface is very smooth, and the fractured paths of river line patterns can be observed, which is indicative of brittle fracture. It can be observed in epoxy/nano-silica composites (series "b, c, d, and e") that the nano-silica particles are embedded in the epoxy matrix other than naked outside, and there is no evidence of particle-matrix debonding in all the figures, which suggests the relatively strong interfacial bonding and excellent compatibility of nano-silica particles with the epoxy matrix.[31] Thereby, the enhancement effect is mainly determined by the volume fraction and dispersion of the nano-silica particles. In the case of epoxy with low nano-silica loadings (series "b, c, and d"), the nano-silica particles are observed to be homogenously dispersed in less than 1 μm scales inside the epoxy matrix. The fractured surfaces are rough, and the fractured paths are radically aligned around the nano-silica particles centers [as

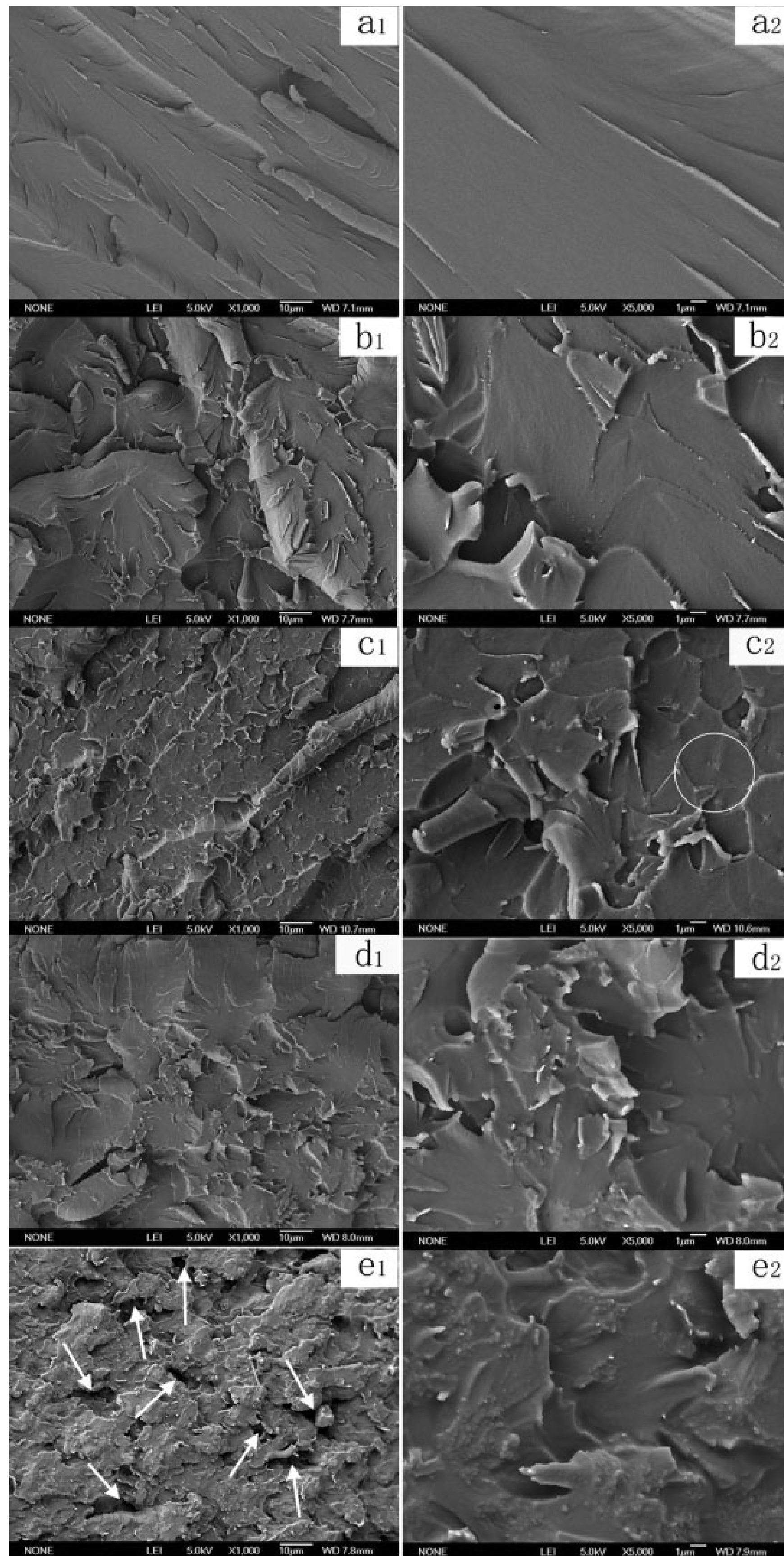

Figure 10 SEM micrographs (series "1" and "2" for different magnifications) of epoxy with (a) 0 wt %; (b) 1 wt %; (c) 2 wt %; (d) 3 wt %; and (e) 5 wt % nano-silica loadings, arrows in (e_1) point to holes and cavities.

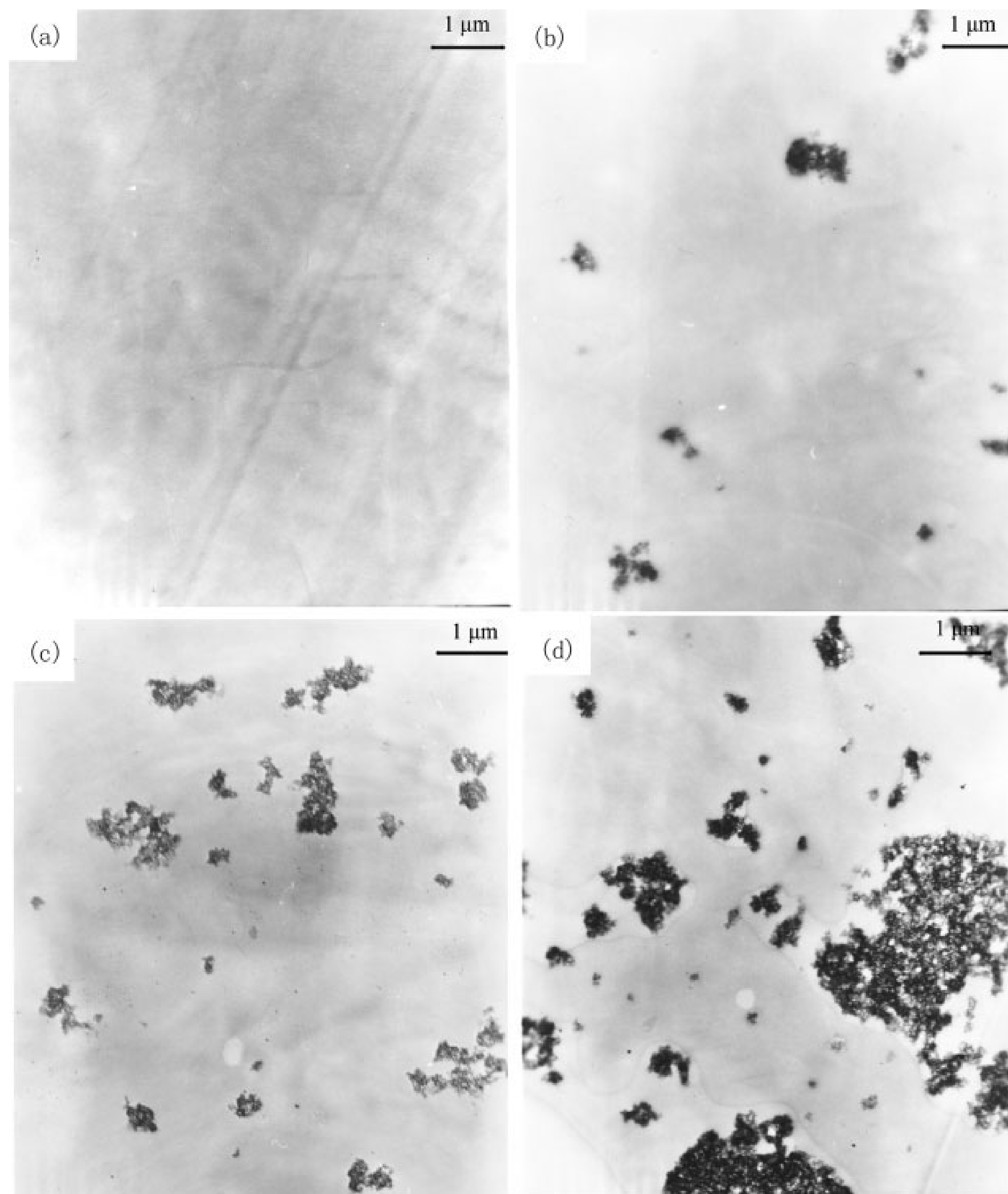

Figure 11 TEM micrographs for epoxy with (a) 0 wt %; (b) 2 wt %; (c) 3 wt %; and (d) 5 wt % nano-silica loadings.

specially marked in Fig. 10(c_2)]. This demonstrates that the nano-silica particles can act as stress concentrators to absorb some of the impact energy and contribute to the enhancement. However, in the case of series "e," nano-silica particle aggregations of up to several microns are observed. Besides, holes and cavities [indicated by arrows in Fig. 10(e_1)] are also observed in the fractured surface which may probably be caused by water or other small molecular chemical compounds adhered to the nano-silica particles. The aggregations of nano-silica particles and the defects in microstructures might be the main explanations to the decrease in toughness.

The dispersion of nano-silica particles in the composites are further characterized and proved by TEM analysis (Fig. 11). It is observed that in the composites with nano-silica loadings of 2 and 3 wt %, the particles are well dispersed with aggregations less than 1 μm, whereas aggregations up to several microns are observed in the composites with 5 wt % of nano-silica loading. This is in accordance with the SEM results.

CONCLUSIONS

Nano-silica particles have been introduced into epoxy resin to achieve good toughness and mechanical strength. The results have shown that with the incorporation of GPDMS, the nano-silica particles exhibited good compatibility with the epoxy matrix, and the enhancement is determined by the concentration and dispersion of nano-silica particles. Both flexural

strength and the fracture toughness have been improved with the incorporation of nano-silica and the sample containing 3 wt % of nano-silica particles have displayed the highest fracture toughness. The addition of nano-silica particles is found to induce slight changes in the curing reaction, the glass transition temperature, and the insulating properties. The nano-silica have been used without any surface treatment, thereby a lot of —OH groups and other small molecules are adhered on the surface of the nano-silica particles. The existence of such —OH groups and small molecules causes a decrease in the activation energy of the curing reaction. It also contributes to the increase in the DC conductivity and the dielectric loss.

References

1. Chikhi, N.; Fellahi, S.; Bakar, M. Eur Polym Mater 2002, 38, 251.
2. Stone, G. C.; Boulter, E. A. Electrical Insulation for Rotating Machines; Wiley: New Jersey, 2004.
3. David, C. M. Y.; Vincent, C.; Liu, Z. G.; Han, J. In: Industry Applications Conference 2004 39th IAS Annual Meeting Conference Record of the 2004 IEEE 2004, 2, 763.
4. Tareev, B. M. Physics of Dielectric Materials; Mir Publishers: Moscow, 1975.
5. Wetzel, B.; Rosso, P.; Haupert, F.; Friedrich, K. Eng Fract Mech 2006, 73, 2375.
6. Ratna, D.; Manoj, N. R.; Varley, R.; Raman, R. K. S.; Simon, G. P. Polym Int 2003, 52, 1403.
7. Ragosta, G.; Abbate, M.; Musto, P.; Scarinzi, G.; Mascia, L. Polymer 2005, 46, 10506.
8. Seo, K. S.; Kim, D. S. Polym Eng Sci 2006, 46, 1318.
9. Rosso, P.; Ye, L.; Friedrich, K.; Sprenger, S. J Appl Polym Sci 2006, 101, 1235.
10. Deng, S. Q.; Ye, L.; Friedrich, K. J Mater Sci 2007, 42, 2766.
11. Wang, K.; Chen, L.; Wu, J. S.; Toh, M. L.; He, C. B.; Yee, A. F. Macromolecules 2005, 38, 788.
12. Zilg, C.; Mulhaupt, R.; Finter, J. Macromol Chem Phys 1999, 200, 661.
13. Becker, O.; Varley, R.; Simon, G. Polymer 2002, 43, 4365.
14. Ho, T. H.; Leu, T. S.; Sun, Y. M.; Shieh, J. Y. Polym Degrad Stabil 2006, 91, 2347.
15. Wan, M. X.; Li, J. C. J Polym Sci Pol Chem 1998, 36, 2799.
16. Bahar, T.; Celebi, S. S. J Appl Polym Sci 1999, 72, 69.
17. Gonon, P.; Sylvestre, A.; Teysseyre, J.; Prior, C. J Mater Sci Mater El 2001, 12, 81.
18. Liu, Y. L.; Li, S. H. J Appl Polym Sci 2005, 95, 1237.
19. Gonis, J.; Simon, G. P.; Cook, W. D. J Appl Polym Sci 1999, 72, 1479.
20. Navabpour, P.; Nesbitt, A.; Mann, T.; Day, R. J. J Appl Polym Sci 2054 2007, 104.
21. Kissinger, H. E. Anal Chem 1957, 29, 1702.
22. Lu, C. L.; Cui, Z. C.; Yang, B.; Su, X. P.; Huo, C. S.; Shen, J. C. J Appl Polym Sci 2002, 86, 589.
23. Ozawa, T. Bull Chem Soc Jpn 1965, 38, 835.
24. Flynn, J H. J Therm Anal 1991, 37, 193.
25. Sun, G.; Sun, H. G.; Liu, Y.; Zhao, B. Y.; Zhu, N.; Hu, K. Polymer 2007, 48, 330.
26. Arora, S. K.; Patel, V.; Kothari, A. Mater Chem Phys 2004, 84, 323.
27. Mark, J.; Ngai, K.; Graessley, W.; Mandelkern, L.; Samulski, E.; Koenig, J.; Wignall, G. Physical Properties of Polymers; Cambridge university press: New York, 2004.
28. Hutchinson, J. M. J Therm Anal Calorim 2003, 72, 619.
29. Liu, Y. H.; Zheng, S. X.; Nie, K. M. Polymer 2005, 46, 12016.
30. Zhu, Y. T.; Cheng, C.; Jin, W. F.; Xie, H. K.; Liu, Y. N. In: International Symposium on Electrical Insulating Materials, 17–20 September, 1995, pp 77–80.
31. Wang, H. Y.; Bai, Y. L.; Liu, S.; Wu, J. L.; Wong, C. P. Acta Mater 2002, 50, 4369.